

MODELS FOR INFORMATION PROPAGATION ON GRAPHS

OLIVER R. A. DUNBAR, CHARLES M. ELLIOTT AND LISA MARIA KREUSSER

ABSTRACT. In this work we propose and unify classes of different models for information propagation over graphs. In a first class, propagation is modeled as a wave which emanates from a set of *known* nodes at an initial time, to all other *unknown* nodes at later times with an ordering determined by the time at which the information wave front reaches nodes. A second class of models is based on the notion of a travel time along paths between nodes. The time of information propagation from an initial *known* set of nodes to a node is defined as the minimum of a generalized travel time over subsets of all admissible paths. A final class is given by imposing a local equation of an eikonal form at each *unknown* node, with boundary conditions at the *known* nodes. The solution value of the local equation at a node is coupled the neighbouring nodes with smaller solution values. We provide precise formulations of the model classes in this graph setting, and prove equivalences between them. Motivated by the connection between first arrival time model and the eikonal equation in the continuum setting, we demonstrate that for graphs in the particular form of grids in Euclidean space mean field limits under grid refinement of certain graph models lead to Hamilton-Jacobi PDEs. For a specific parameter setting, we demonstrate that the solution on the grid approximates the Euclidean distance.

1. INTRODUCTION

In this work, we formulate models for information propagation on a graph inspired by the modelling of waves passing through continuous media. Consider an open bounded domain $\Omega \subset \mathbb{R}^d$ for $d \geq 1$ with a Lipschitz boundary Γ , a given point $x_0 \in \Omega$ and a continuous, positive function $s: \bar{\Omega} \rightarrow \mathbb{R}$. A first approach proposes a propagating front separating the region for which the wave has arrived from the remainder. The fronts initiate at x_0 , and are characterised by being level surfaces of the arrival time from x_0 . Here $s(x)$ controls the additional time for the front to travel through the medium at x .

A second classical approach consists of formulating a model based on finding the smallest travel time over a set of possible paths. The aim of this model is to determine the shortest travel time along any path from x_0 to every $x \in \bar{\Omega}, x \neq x_0$, in the medium $\bar{\Omega}$ for a given impedance s . This task can be expressed as the minimisation problem

$$u(x) = \inf_{\substack{\xi \in W^{1,\infty}([0,1], \bar{\Omega}), \\ \xi(0)=x_0, \quad \xi(1)=x}} \left\{ \int_0^1 s(\xi(r)) \|\xi'(r)\|_2 \, dr \right\}, \quad (1.1)$$

cf. [8], where $\|\cdot\|_2$ denotes the 2-norm in \mathbb{R}^d and $\xi(\cdot)$ is a parameterised path in the Sobolev space $W^{1,\infty}$. Since large values of s slow down the movement and increase the travel time within the medium, we sometimes refer to s as the slowness function, while its inverse $\frac{1}{s}$ can be regarded as a velocity.

A third approach arises because an optimal value u for (1.1) is a solution to the eikonal equation, an isotropic static Hamilton-Jacobi partial differential equation. The eikonal equation is given by

$$\|\nabla u\|_2 = s \quad \text{in } \Omega \setminus \{x_0\} \quad (1.2)$$

with boundary conditions

$$\begin{aligned} u(x_0) &= 0, \\ \nabla u(x) \cdot \nu(x) &\geq 0 \quad \text{for } x \in \Gamma, \end{aligned} \quad (1.3)$$

where ν is the unit outer normal to Γ .

These three approaches of wave propagation in continuum settings have been exploited to advance different fields of research. For instance, (i) the optimization over paths arises in modelling

many applications, (ii) the study of the eikonal equation leads to existence and uniqueness theory, and (iii) efficient numerical methods take advantage of propagating wave fronts by fast marching algorithms for solving the continuum eikonal equation, [21, 22].

The aim of this work is to propose and unify corresponding perspectives in the graph setting. We formulate several classes of models and relate them to each other. We begin with a class of front propagation models. A second class considers the smallest arrival time over sets of admissible paths. The final class formulates a local equation for the relation between arrival times for a node and its neighbours similar to the eikonal equation in the continuum setting. We prove the equivalence of the models for special cases. In certain cases of graphs corresponding to regular grids in Euclidean space we derive formal PDE limits. We also provide some computational examples illustrating the models.

Applications frequently involve data defined on complex spaces such as network-like structures or point clouds that may be represented as graphs. Processing and analysing complex data poses a challenging task, especially in high dimensional settings. Many computational methods for semi-supervised and unsupervised classification are based on variational models and PDEs. Examples include algorithms based on phase fields [3] and the MBO scheme [19], as well as p -Laplacian equations [16]. It is natural to introduce the concept of information propagation to data classification and semi-supervised learning [4, 2, 25, 18]. The success of eikonal equations in the continuum setting motivates the development of similar tools on graphs. In a series of papers, Elmoataz et al. [9, 10, 15, 23] postulate discrete eikonal equations and investigate label propagation on graphs with applications in imaging and machine learning. Current analytical results include an investigation of viscosity solutions for Hamilton-Jacobi equations on networks [6] and an approximation scheme for an eikonal equation on a network [5], producing an approximation of shortest paths to the boundary. In addition, limits and consistency of non-local and graph approximations to the time-dependent (local) eikonal equation have been studied in [17].

1.1. Outline. We introduce several models for travel times on a graph in Section 2. Equivalences between certain instances of the models are established in Section 3. In Section 4, we derive Hamilton-Jacobi equations of eikonal type as mean field limits on structured graphs. We illustrate the models in Section 5 by considering different computational examples, both from the setting of regular grids and random graphs.

1.2. Notation. Following the terminology and setting in [13, 15, 18], we consider a finite, undirected, connected weighted graph $G = (V, E, w)$ with vertices $V = \{1, \dots, n\}$, edges $E \subset V^2$ and nonnegative edge weights w . We assume that the graph is simple, i.e. there exists at most one edge between any two vertices. We suppose that there is a decomposition of $V := \partial V \cup \mathring{V}$ into two disjoint non-empty sets ∂V and \mathring{V} .

The edge between node i and node j is denoted by (i, j) . For ease of notation, we regard the weights w as a weight matrix $w \in \mathbb{R}^{n \times n}$ with entries w_{ij} , where we assume that there exists an edge $(i, j) \in E$ if and only if $w_{ij} > 0$, while $w_{ij} = 0$ if $(i, j) \notin E$. Since G is an undirected graph, we have $w_{ij} = w_{ji}$ and hence w is a symmetric matrix. This framework also includes unweighted graphs corresponding to the cases in which $w_{ij} = 1$ for all $(i, j) \in E$.

Given a graph G , we denote by $N(i) \subset V$ the set of neighbours of node $i \in V$, i.e. for each $j \in N(i)$ there exists an edge $(i, j) \in E$. We introduce the notion of a path from node $x \in V$ to $y \in V$ and write $p_{x,y} = (x = i_1, \dots, y = i_{n(p_{x,y})})$ for a path with $n(p_{x,y})$ nodes and $n(p_{x,y}) - 1$ edges $(i_{m-1}, i_m) \in E$ for $m = 2, \dots, n(p_{x,y})$ such that all nodes i_m for $m \in \{1, \dots, n(p_{x,y})\}$ are distinct, i.e. a path must not self-intersect. Due to the assumption that the graph G is connected, for every $x, y \in V$ there exists a path $p_{x,y}$ connecting x and y , i.e. there exists $n(p_{x,y}) > 1$ such that $p_{x,y} = (x = i_1, \dots, y = i_{n(p_{x,y})})$ is a path with edges $(i_{m-1}, i_m) \in E$ for $m = 2, \dots, n(p_{x,y})$.

Given a graph with $|V| = n$ nodes, we denote by \mathcal{H}^n the function space of all functions defined on V , i.e. all $v \in \mathcal{H}^n$ are of the form $v: V \rightarrow \mathbb{R}$. For $v \in \mathcal{H}^n$, we write $v_x = v(x)$ for $x \in V$. We also assume that there is a given *slowness* function $s \in \mathcal{H}^n$ with $s \geq 0$.

2. DESCRIPTION OF MODELS

In this section, we propose several models for the propagation of information on graphs. The common elements of the models are:

- We suppose that either all information has arrived at a vertex or none.
- We introduce the variable $u \in \mathcal{H}^n$ with u_i for $i \in V$ to denote the *arrival time* of information at vertex i .
- We assume that u is prescribed on ∂V and we set $u = 0$ on ∂V , though in general the models can accommodate a wider class of boundary conditions.
- We suppose that information propagation is local. That is, information arrives at a vertex only by propagation from a neighbouring vertex for which information has arrived. Thus there is a unique travel time u_i at each node i that can only depend on travel times at nodes $j \in N(i)$ with $u_j < u_i$.
- The edge weights reflect the distance or resistance to propagation along an edge.
- The function $s \in \mathcal{H}^n$ is a measure of slowness or resistance associated with each vertex.

The aim of a model is to associate a travel time u_i with each vertex of the graph. Since the graph is finite, $u = \{u_i, i = 1, 2, \dots, n\}$ attains an unknown number of $L + 1 \in \mathbb{N}$ distinct values consisting of prescribed initial data $U_0 \in \mathbb{R}$ and unknown values $U_1, \dots, U_L \in \mathbb{R}$ ordered so that $U_0 < \dots < U_L$. We set $V_0 := \partial V$ as the set of initially labelled vertices and prescribe the initial data U_0 , i.e. $u_i = U_0$ for all $i \in V_0$. In the following we set $U_0 = 0$.

We consider three classes of models in this section. The first class of models is based on the propagation of discrete fronts from an initial front ∂V (Model 1). The second class of models considers first arrival times of sets of paths that link vertices in the initial set ∂V to vertices in $\dot{V} = V \setminus \partial V$ (Model 2). For the third class of models, we postulate a generalized discrete eikonal equation model (Model 3).

2.1. Front propagation models. In this approach, we view propagation of information as an evolving front. We decompose the set \dot{V} of initially unlabelled vertices into L disjoint sets V_1, \dots, V_L such that for $j \in \{1, \dots, L\}$ all vertices $i \in V_j$ satisfy $u_i = U_j$. We define *known* sets K_0, \dots, K_L and *candidate* sets C_0, \dots, C_L as follows:

$$K_l = \bigcup_{j \in \{0, \dots, l\}} V_j, \quad C_l = \bigcup_{j \in K_l} N(j) \setminus K_l.$$

Under the assumption that U_j and V_j for $j = 0, \dots, k-1$ are known, implying that the value of u_i for all $i \in K_{k-1}$ is known, our task is to determine U_k and V_k . The front F_{k-1} consists of all vertices in K_{k-1} with neighbours in C_{k-1} and with $F_0 = V_0$. We determine candidate values \tilde{u}_i for each $i \in C_{k-1}$ using a model (specified below) and we define U_k by choosing the smallest candidate value in the candidate set C_{k-1} :

$$U_k := \min_{i \in C_{k-1}} \tilde{u}_i. \quad (2.1)$$

We then define $V_k \subset C_{k-1}$ to be the set where the minimum is attained and we set $u_i = U_k$ for all $i \in V_k$.

The above procedure depends on the definition of candidate values \tilde{u}_i for $i \in C_{k-1}$. We define relationships for \tilde{u}_i that depend upon the set $N(i) \cap K_{k-1}$. Using (2.1), the values U_1, \dots, U_L of the solution u can then be determined.

2.1.1. Model 1(i). Given the known arrival time u_j for $j \in K_{k-1}$, a possible candidate for the arrival time at $i \in N(j)$ via edge (j, i) is given by $u_j + \frac{s_i}{w_{j,i}}$. Choosing the smallest value of all these possible candidate values results in the candidate

$$\tilde{u}_i = \min_{j \in N(i) \cap K_{k-1}} \left\{ u_j + \frac{s_i}{w_{j,i}} \right\} \quad (2.2)$$

for $i \in C_{k-1}$. Here, $u_j + \frac{s_i}{w_{j,i}}$ is the sum of the first arrival time u_j at node j and $\frac{s_i}{w_{j,i}}$ which is the travel time from j to i along edge (j, i) . The travel time along (j, i) only depends on the slowness s_i at the endpoint of (j, i) and the edge weight $w_{j,i}$. The term $\frac{s_i}{w_{j,i}}$ is inspired from the continuum

setting (1.1) which suggests that the travel time along an edge (i, j) is antiproportional to the velocity $\frac{1}{s_i}$ and hence proportional to s_i . (1.1) also suggests that the travel time is proportional to the length of an edge and thus proportional to $\frac{1}{w_{i,j}}$ if we regard $w_{i,j}$ as a characterisation of the connectivity of vertices i and j .

2.1.2. Model 1(ii). We define $z_i^2 := \sum_{j \in N(i) \cap K_{k-1}} w_{i,j}^2$ for $i \in C_{k-1}$, i.e. $z_i^2 = \|(w_{i,j})_{j \in N(i) \cap K_{k-1}}\|_2^2$. For $i \in C_{k-1}$, we set

$$\tilde{u}_i = \mu_i + \sqrt{\frac{s_i^2}{z_i^2} - \sigma_i^2}. \quad (2.3)$$

Here,

$$\mu_i = \frac{1}{z_i^2} \sum_{j \in N(i) \cap K_{k-1}} w_{i,j}^2 u_j$$

is the weighted mean travel time to any $j \in N(i) \cap K_{k-1}$ with $\frac{1}{z_i^2} \sum_{j \in N(i) \cap K_{k-1}} w_{i,j}^2 = 1$ and

$$\sigma_i^2 = \sum_{j \in N(i) \cap K_{k-1}} \left(\frac{w_{i,j}^2}{z_i^2} u_j^2 \right) - \mu_i^2$$

is its variance. Note that σ_i vanishes if $u_j = \mu_i$ for all $j \in N(i) \cap K_{k-1}$. Further, since $s_i > 0$, we have

$$\sqrt{\frac{s_i^2}{z_i^2}} = \frac{s_i}{\|(w_{i,j})_{j \in N(i) \cap K_{k-1}}\|_2},$$

which is of a similar form as the travel time from $j \in N(i)$ to i in (2.2) and can be regarded as a weighted travel time from $N(i) \cap K_{k-1}$ to i .

2.1.3. Model 1(iii). We define $M_{i,k} = \sum_{j \in N(i) \cap K_{k-1}} w_{i,j}$ and $y_i := \sum_{j \in N(i) \cap K_{k-1}} w_{i,j}$ for $i \in C_{k-1}$, i.e. $y_i = \|(w_{i,j})_{j \in N(i) \cap K_{k-1}}\|_1$. We set

$$\tilde{u}_i = \frac{1}{y_i} \sum_{j \in N(i) \cap K_{k-1}} (w_{i,j} u_j) + \frac{s_i}{y_i} = \frac{1}{y_i} \sum_{j \in N(i) \cap K_{k-1}} w_{i,j} \left(u_j + \frac{s_i}{M_{i,k} w_{i,j}} \right) \quad (2.4)$$

for $i \in C_{k-1}$. We may interpret this as a weighted mean travel time over all the determined neighbours in which the resistance is divided equally to each edge.

2.2. First arrival times. In this approach, we optimize travel times over path sets. For this, we define useful quantities for describing path sets. Then, we define some generalized travel time models and first arrival times over path sets. In Remark 2.1 we show how this generalizes the more familiar travel time defined over paths.

For two nodes $x_0, i \in V$, let $\mathbb{P}_{x_0,i}$ be the set of admissible paths $p_{x_0,i}$ from x_0 to i . Since the graph $G = (V, E, w)$ is connected, $\mathbb{P}_{x_0,i}$ is non-empty. Let $P_{x_0,i} \subset \mathbb{P}_{x_0,i}$ denote a non-empty subset of paths from x_0 to i and we refer to $P_{x_0,i}$ as a *path set*. We define the *penultimate truncation of a path* $p_{x_0,i} \in \mathbb{P}_{x_0,i}$ as a path $p_{x_0,j}$, where $j \in N(i)$ and $p_{x_0,i} = (p_{x_0,j}, (j, i))$. Similarly, for a path set $P_{x_0,i}$, we define the *penultimate truncations of $P_{x_0,i}$* as the set $\{p_{x_0,j} : j \in K(P_{x_0,i})\}$ where $K(P_{x_0,i}) \subset N(i)$ such that for every $j \in K(P_{x_0,i})$ there exist a path $p_{x_0,j}$ and a path $p_{x_0,i} \in P_{x_0,i}$ such that $p_{x_0,i} = (p_{x_0,j}, (j, i))$. Note, unlike the set $N(i)$ which depends only on the graph structure, $K(P_{x_0,i})$ depends on the choice of the path set $P_{x_0,i}$. An illustration of a path set and its penultimate truncation is shown in Figure 1.

We assume that there exists a formula for a generalised travel time $T(Q)$ for any path set $Q \subset \mathbb{P}_{x_0,i}$. Some specific examples are introduced below. We define u_i for $i \in V$, as the first arrival travel times over path sets by

$$u_i = \min_{x_0 \in \partial V} \min_{P_{x_0,i} \subset \mathbb{P}_{x_0,i}} T(P_{x_0,i}). \quad (2.5)$$

For boundary nodes $x_0 \in \partial V$, we set $u_{x_0} = 0$. The inner minimization in (2.5) is not over paths $p_{x_0,i} \in \mathbb{P}_{x_0,i}$, but over *path sets* $P_{x_0,i} \subset \mathbb{P}_{x_0,i}$.

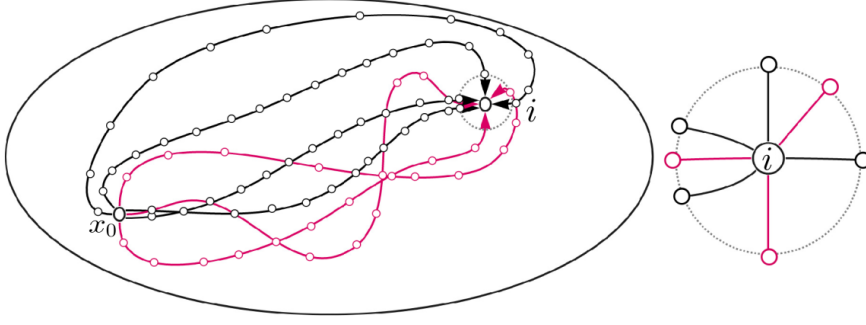


FIGURE 1. An illustration of a path set and its truncation. On the left we represent the set of all paths $\mathbb{P}_{x_0, i}$ between two nodes x_0 and i with black arrows from x_0 to i . We represent a path set $P_{x_0, i} \subset \mathbb{P}_{x_0, i}$ in pink. In particular the path set $P_{x_0, i}$ contains three paths. On the right of the figure, we zoom into the neighbourhood $N(i)$, represented as nodes on dotted circle; the pink nodes on the dotted circle represent the penultimate truncation $K(P_{x_0, i}) \subset N(i)$ of the path set. The pink edges therefore can be written as (j, i) such that $j \in K(P_{x_0, i})$.

We define a travel time T over a path set $P_{x_0, i}$ with a local formula over the penultimate truncations of $P_{x_0, i}$. In particular $T(P_{x_0, i})$ is calculated as a function of $T(P_{x_0, j}^i)$ with $j \in K(P_{x_0, i})$ where

$$P_{x_0, j}^i = \{p_{x_0, j} \in \mathbb{P}_{x_0, j} : (p_{x_0, j}, (j, i)) \subset P_{x_0, i}\}.$$

By definition $P_{x_0, j}^i$ is also a path set. Since all nodes of a path are distinct by definition, for all $p_{x_0, j} \in P_{x_0, j}^i$ we have $i \notin p_{x_0, j}$.

The models we propose share similarities with the front propagation models 1(i), 1(ii), 1(iii) in Section 2.1 and are specified further below.

2.2.1. Model 2(i). Similar to Model 1(i) in (2.2), we define

$$T(P_{x_0, i}) = \min_{j \in K(P_{x_0, i})} \left\{ T(P_{x_0, j}^i) + \frac{s_i}{w_{j, i}} \right\}. \quad (2.6)$$

2.2.2. Model 2(ii). Similar to Model 1(ii) in (2.3), we consider

$$T(P_{x_0, i}) = \mu_{x_0, i} + \sqrt{\frac{s_i^2}{z_{x_0, i}} - \sigma_{x_0, i}^2}, \quad (2.7)$$

where

$$z_{x_0, i} = \sum_{j \in K(P_{x_0, i})} w_{j, i}^2,$$

$$\mu_{x_0, i} = \frac{1}{z_{x_0, i}} \sum_{j \in K(P_{x_0, i})} w_{j, i}^2 T(P_{x_0, j}^i)$$

and

$$\sigma_{x_0, i}^2 = \sum_{j \in K(P_{x_0, i})} \left(\frac{w_{j, i}^2}{z_{x_0, i}} (T(P_{x_0, j}^i))^2 \right) - \mu_{x_0, i}^2.$$

2.2.3. Model 2(iii). Similar to Model 1(iii) in (2.4), we define $y_{x_0,i} = \sum_{j \in K(P_{x_0,i})} w_{j,i}$ and

$$T(P_{x_0,i}) = \frac{1}{y_{x_0,i}} \sum_{j \in K(P_{x_0,i})} w_{j,i} T(P_{x_0,j}^i) + \frac{s_i}{y_{x_0,i}}. \quad (2.8)$$

Due to the assumption that the graph G is connected and the weights $w_{i,j}$ are positive, there exists a solution to (2.5). Clearly first arrival time solutions are well-defined and unique. However, the minimising path sets are not unique in general.

Remark 2.1. Consider a singleton path set $P_{x_0,i} = \{p_{x_0,i}\} = \{(x_0 = i_1, \dots, i = i_M)\}$. We observe that the value of $T(P_{x_0,i})$ calculated using models 2(i), 2(ii), or 2(iii), is equal to the following:

$$T(\{p_{x_0,i}\}) = T(\{p_{x_0,i_{M-1}}\}) + \frac{s_{i_M}}{w_{i_{M-1},i_M}} = T(\{p_{x_0,i_{M-1}}\}) + T(\{(i_{M-1}, i_M)\}) = \sum_{m=2}^M T(\{(i_{m-1}, i_m)\}), \quad (2.9)$$

where we used that the models 2(i), 2(ii), and 2(iii) satisfy

$$T(\{(i_{m-1}, i_m)\}) = \frac{s_{i_m}}{w_{i_{m-1},i_m}}. \quad (2.10)$$

If we suppose that w_{i_{m-1},i_m} characterises the connectivity between nodes i_{m-1} and i_m , and thus $\frac{1}{w_{i_{m-1},i_m}}$ is proportional to the travel time, the form of the travel time (2.9) can be regarded as a discretisation of $\int_0^1 s(\xi(r)) \|\xi'(r)\|_2 dr$ in (1.1).

Classically, there is a known relationship between the discretisation of problem (1.1) and the minimization problem

$$u_i = \min_{x_0 \in \partial V} \min_{p_{x_0,i} \in \mathbb{P}_{x_0,i}} T(\{p_{x_0,i}\}), \quad (2.11)$$

where $u_{x_0} = 0$ on boundary nodes $x_0 \in \partial V$. Under the assumption that only singleton sets $P_{x_0,i} = \{p_{x_0,i}\}$ may be considered in (2.5), then (2.5) reduces to (2.11).

To understand the behaviour of model 2(i) in (2.6), substituting its definition in (2.5), we obtain (2.11). Indeed,

$$\begin{aligned} u_i &= \min_{x_0 \in \partial V} \min_{P_{x_0,i} \subset \mathbb{P}_{x_0,i}} \min_{j \in K(P_{x_0,i})} \left\{ T(P_{x_0,j}^i) + \frac{s_i}{w_{j,i}} \right\} \\ &= \min_{x_0 \in \partial V} \min_{j \in K(\mathbb{P}_{x_0,i})} \left\{ T(P_{x_0,j}^i) + \frac{s_i}{w_{j,i}} \right\} \\ &= \min_{x_0 \in \partial V} T(\mathbb{P}_{x_0,i}) \\ &= \min_{x_0 \in \partial V} \min_{p_{x_0,i} \in \mathbb{P}_{x_0,i}} T(\{p_{x_0,i}\}). \end{aligned}$$

Thus, when using model 2(i), a minimization over path sets is thus reduced to a minimization over paths.

To understand the behaviour of models 2(ii) and 2(iii), we calculate the generalised travel time of some simple path sets over the square grid in two space dimensions with constant unit weights and slowness function; see Figures 2 and 3, respectively. In each case, we calculate the travel times for the three path sets $P_{x_0,i}^{(1)}$, $P_{x_0,i}^{(2)}$ and $P_{x_0,i}^{(3)}$, where $x_0 = (0,0)$ and $i = (2,2)$. Let U and R be the paths travelling ‘up’ and ‘right’ from a node to a neighbour on the square grid. We set $P_{x_0,i}^{(1)} = \{(U, R, U, R)\}$, $P_{x_0,i}^{(2)} = P_{x_0,i}^{(1)} \cup \{(R, U, R, U)\}$ and $P_{x_0,i}^{(3)} = P_{x_0,i}^{(2)} \cup \{(U, U, R, R), (R, R, U, U)\}$, so these path sets have 1, 2 and 4 elements, respectively. We show the generalised travel time for path sets $P_{x_0,i}^{(1)}$, $P_{x_0,i}^{(2)}$ and $P_{x_0,i}^{(3)}$ for models 2(ii) and 2(iii) in Figures 2 and 3, respectively. Here, the numbers at nodes along the different paths denote the generalised travel time from the origin x_0 to the respective nodes. We see that $P_{x_0,i}^{(3)}$ is optimal for model 2(ii) and 2(iii) among $\{P_{x_0,i}^{(1)}, P_{x_0,i}^{(2)}, P_{x_0,i}^{(3)}\}$ as shown in Figures 2 and 3. In fact, $P_{x_0,i}^{(3)}$ is an optimal path set for model 2(ii) and 2(iii) among all subsets of $\mathbb{P}_{x_0,i}$ on the square grid.

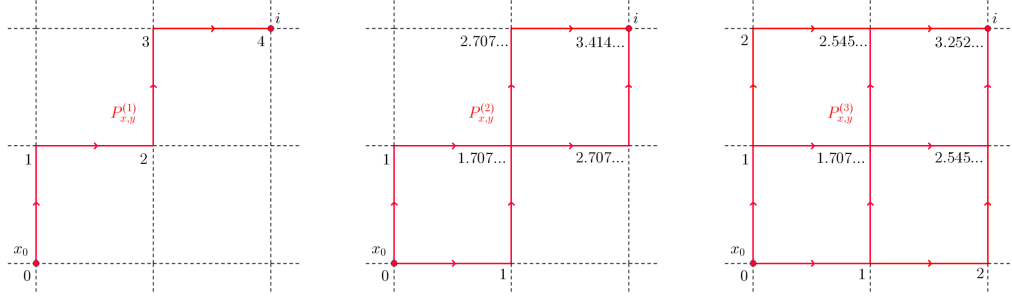


FIGURE 2. Three different path sets shown in red on a square grid with $w_{i,j} = 1$ and $s_i = 1$ for all nodes. The numbers correspond to the values of the generalized travel time $T(P^{(i)}_{x_0,i})$ for model 2(ii) for each path set.

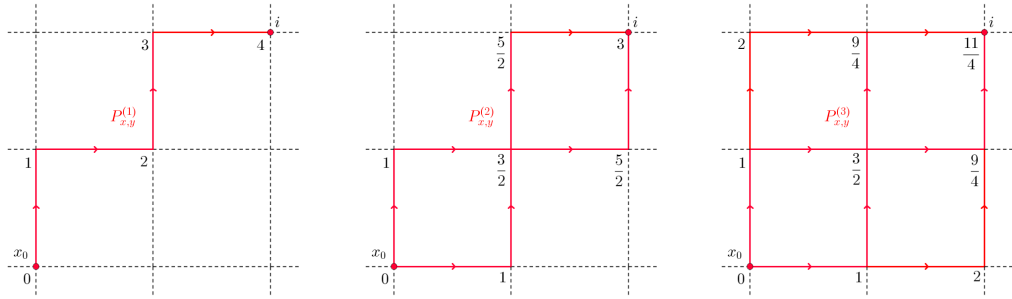


FIGURE 3. Three different path sets shown in red on a rectangular grid with $w_{i,j} = 1$ and $s_i = 1$ for all nodes. The numbers correspond to the values of the generalized travel time $T(P^{(i)}_{x_0,i})$ for model 2(iii) for each path set.

The properties of minimizing path sets are left to future investigation. Heuristically we see that the travel times given by model 2(ii) or 2(iii) are small for path sets that contain short paths or paths which have many cross-overs among themselves (i.e. multiple distinct paths pass through common nodes). Such behaviour is observed in Figures 2 and 3, where the support of the minimizing paths is the rectangular lattice between nodes x_0 and i .

Remark 2.2. The notion of a minimising path in (2.5) also includes the case of a single element of ∂V which corresponds to one label, i.e. $\partial V = \{x_0\}$ in which case

$$u_i = \min_{P_{x_0,i} \subset \mathbb{P}_{x_0,i}} T(P_{x_0,i}).$$

2.3. Discrete generalised eikonal models. For this model class, we postulate a discrete generalized eikonal equation. For $i \in V$, we define one sided edge derivatives $\nabla_w^+ u_i \in \mathbb{R}^{|N(i)|}$ by

$$\nabla_w^+ u_i = (w_{j,i}(u_i - u_j)^+)_{j \in N(i)}.$$

Then,

$$\|\nabla_w^+ u_i\|_p = \left(\sum_{j \in N(i)} (w_{j,i}(u_i - u_j)^+)^p \right)^{1/p} \quad (2.12)$$

for $1 \leq p < \infty$, and

$$\|\nabla_w^+ u_i\|_\infty = \max_{j \in N(i)} \{w_{j,i}(u_i - u_j)^+\}. \quad (2.13)$$

2.3.1. Model 3(p). Motivated by monotone discretisations of the continuum eikonal equation, we consider

$$\begin{aligned} \|\nabla_w^+ u_i\|_p &= s_i, & i \in \mathring{V}, \\ u_i &= 0, & i \in \partial V, \end{aligned} \tag{2.14}$$

for any $1 \leq p \leq \infty$. Note that (2.14) with $p = 2$ is of the same form as the continuum eikonal equation (1.2). We can rewrite (2.14) as

$$\begin{aligned} \sum_{j \in N(i)} (w_{j,i}(u_i - u_j)^+)^p &= s_i^p, & i \in \mathring{V}, \\ u_i &= 0, & i \in \partial V, \end{aligned} \tag{2.15}$$

for $1 \leq p < \infty$, and

$$\begin{aligned} \max_{j \in N(i)} \{w_{j,i}(u_i - u_j)^+\} &= s_i, & i \in \mathring{V}, \\ u_i &= 0, & i \in \partial V, \end{aligned} \tag{2.16}$$

for $p = \infty$. Note that (2.15) satisfies a monotonicity condition characteristic of discrete Hamilton-Jacobi equations (c.f. [8]), implying that the boundary value problem (2.14) has a unique solution [9].

3. RELATIONS BETWEEN MODELS

In this section, we investigate relations between the different modelling approaches, that is front propagation, first arrival time and discrete eikonal models, which are introduced in Section 2. The relationships we prove between the models are summarised in Table 1.

Front propagation	First arrival	Discrete eikonal
Model 1(i)	Model 2(i)	Model 3($p = \infty$)
Model 1(ii)	Model 2(ii)	Model 3($p = 2$)
Model 1(iii)	Model 2(iii)	Model 3($p = 1$)

TABLE 1. We summarize proved equivalences between the front propagation, arrival time (path and path set) and discrete eikonal models.

3.1. Equivalence of front propagation and discrete eikonal models. In this section, we show the equivalence of front propagation models (2.2), (2.3), (2.4) (i.e. models 1(i),(ii),(iii)) and discrete eikonal models (2.15) for $p = 1, p = 2$ and (2.16) for $p = \infty$ (i.e. models 3($p = 1$), 3($p = 2$), 3($p = \infty$)).

3.1.1. Equivalence of Models 1(i) and 3($p = \infty$). Let $i \in \mathring{V}$ be given. Hence, there exists $k \in \{1, \dots, L\}$ such that $i \in V_k$. The definition of model 1(i) in (2.2) is equivalent to

$$u_i = \min_{j \in N(i) \cap K_{k-1}} \left\{ u_j + \frac{s_i}{w_{j,i}} \right\},$$

that is

$$\max_{j \in N(i) \cap K_{k-1}} \left\{ \frac{w_{j,i}(u_i - u_j) - s_i}{w_{j,i}} \right\} = 0.$$

Since $w_{j,i} > 0$ for all edges $(j, i) \in E$, the model is equivalent to

$$\max_{j \in N(i) \cap K_{k-1}} \{w_{j,i}(u_i - u_j) - s_i\} = 0.$$

We have $u_j \geq u_i$ for all $j \in V \setminus K_{k-1}$, while the maximum can only be attained for any $j \in V$ with $u_j < u_i$ since $w_{j,i} > 0$ and $s_i > 0$. The set over which we maximize can be replaced by $N(i)$, i.e.

$$\max_{j \in N(i)} \{w_{j,i}(u_i - u_j)^+ - s_i\} = 0,$$

which is equivalent to (2.16), i.e. model 3($p = \infty$).

3.1.2. Equivalence of Models 1(ii) and 3($p = 2$). Let $i \in \mathring{V}$, that is, there exists $k \in \{1, \dots, L\}$ such that $i \in V_k$. First, we show that model 3($p = 2$) in (2.15) follows from model 1(ii) in (2.3). Since $z_i = \sum_{j \in N(i) \cap K_{k-1}} w_{i,j}^2$, (2.3) is equivalent to

$$\sum_{j \in N(i) \cap K_{k-1}} w_{i,j}^2 u_i = \sum_{j \in N(i) \cap K_{k-1}} w_{i,j}^2 u_j + \sqrt{\left(\sum_{j \in N(i) \cap K_{k-1}} w_{i,j}^2 u_j \right)^2 - z_i \left(\sum_{j \in N(i) \cap K_{k-1}} w_{i,j}^2 u_j^2 - s_i^2 \right)}.$$

For this, we square both sides of the equality which yields

$$(z_i u_i)^2 - 2u_i z_i \sum_{j \in N(i) \cap K_{k-1}} w_{i,j}^2 u_j = z_i s_i^2 - z_i \sum_{j \in N(i) \cap K_{k-1}} w_{i,j}^2 u_j^2.$$

Since $z_i > 0$, we obtain

$$\sum_{j \in N(i) \cap K_{k-1}} w_{i,j}^2 (u_i - u_j)^2 = s_i^2, \quad (3.1)$$

which is equivalent to model 3($p = 2$) in (2.15) due to the definition of K_{k-1} .

Next, we start from model 3($p = 2$) in (2.15) for $p = 2$, or equivalently (3.1), and show that model 1(ii) in (2.3) follows. Note that (3.1) can be regarded as a quadratic equation in u_i whose solution u_i satisfies

$$u_i \in \left\{ \frac{1}{z_i} \left(\sum_{j \in N(i) \cap K_{k-1}} w_{i,j}^2 u_j \pm \sqrt{\left(\sum_{j \in N(i) \cap K_{k-1}} w_{i,j}^2 u_j \right)^2 - z_i \left(\sum_{j \in N(i) \cap K_{k-1}} w_{i,j}^2 u_j^2 - s_i^2 \right)} \right) \right\}.$$

The discriminant is nonnegative due to the existence of a unique real solution to (2.15). Since

$$\frac{1}{z_i} \sum_{j \in N(i) \cap K_{k-1}} w_{i,j}^2 u_j \leq \max_{j \in N(i) \cap K_{k-1}} u_j \leq u_i,$$

this implies that the smaller solution contradicts the definition of $i \in V_k$ and the larger solution of the quadratic equation has to be considered, i.e.

$$u_i = \frac{1}{w_i} \left(\sum_{j \in \tilde{N}(i)} w_{i,j}^2 u_j + \sqrt{\left(\sum_{j \in \tilde{N}(i)} w_{i,j}^2 u_j \right)^2 - w_i \left(\sum_{j \in \tilde{N}(i)} w_{i,j}^2 u_j^2 - s_i^2 \right)} \right),$$

which yields (2.3), that is model 1(ii).

3.1.3. Equivalence of Models 1(iii) and 3($p = 1$). Let $i \in \mathring{V}$ be given. Hence, there exists $k \in \{1, \dots, L\}$ such that $i \in V_k$. Model 1(iii) in (2.4) is equivalent to

$$u_i = \frac{1}{y_i} \left(s_i + \sum_{j \in N(i) \cap K_{k-1}} w_{i,j} u_j \right),$$

which is equivalent to model 3($p = 1$) in (2.15) by the definition of y_i and the properties of $i \in V_k$, i.e.

$$\sum_{j \in N(i)} w_{i,j} (u_i - u_j)^+ = s_i.$$

3.2. Equivalence of first arrival times over path sets and discrete eikonal models. In this section we equate the arrival time model (2.5) with travel times (2.6), (2.7), (2.8) (collectively models 2(i),(ii),(iii)) of Section 2.2 with the discrete eikonal models, i.e. model 3($p = \infty$) in (2.16), and models 3($p = 1$), 3($p = 2$) in (2.15).

3.2.1. Equivalence between Models 2(i) and 3($p = \infty$). Plugging travel time (2.6) of model 2(i) into (2.5) and using the definition of $K(P_{x_0,i})$ for $P_{x_0,i} \subset \mathbb{P}_{x_0,i}$ yields

$$\begin{aligned} u_i &= \min_{x_0 \in \partial V} \min_{P_{x_0,i} \subset \mathbb{P}_{x_0,i}} T(P_{x_0,i}) \\ &= \min_{x_0 \in \partial V} \min_{P_{x_0,i} \subset \mathbb{P}_{x_0,i}} \min_{j \in K(P_{x_0,i})} \left(T(P_{x_0,j}^i) + \frac{s_i}{w_{j,i}} \right) \\ &= \min_{x_0 \in \partial V} \min_{K \subset N(i)} \min_{\{P_{x_0,i} \subset \mathbb{P}_{x_0,i} : K(P_{x_0,i}) = K\}} \min_{j \in K} \left(T(P_{x_0,j}^i) + \frac{s_i}{w_{j,i}} \right) \\ &= \min_{x_0 \in \partial V} \min_{K \subset N(i)} \min_{j \in K} \min_{(P_{x_0,j}^i, (j,i)) \subset \mathbb{P}_{x_0,i}} \left(T(P_{x_0,j}^i) + \frac{s_i}{w_{j,i}} \right) \\ &= \min_{x_0 \in \partial V} \min_{j \in N(i)} \min_{(P_{x_0,j}^i, (j,i)) \subset \mathbb{P}_{x_0,i}} \left(T(P_{x_0,j}^i) + \frac{s_i}{w_{j,i}} \right) \end{aligned}$$

Note that $P_{x_0,j}^i$ contains paths between x_0 and j not containing node i . If we now consider $P_{x_0,j} \subset \mathbb{P}_{x_0,j}$, then there may be a path from x_0 to j via i in $P_{x_0,j}$, but it is not a minimiser. To see that a path $p_{x_0,j}$ with $i \in p_{x_0,j}$ is indeed not a minimiser, we consider $p_{x_0,j} = (i_1 = x_0, \dots, i_k = i, \dots, i_M = j)$ for some $M \in \mathbb{N}$ and $1 < k < M$, implying that $i_{k-1} \in N(i)$ and hence $p_{x_0,i} = (i_1 = x_0, \dots, i_{k-1}, i_k = i) \in (P_{x_0,\tilde{j}}^i, (\tilde{j}, i)) \subset \mathbb{P}_{x_0,i}$ for $\tilde{j} = i_{k-1} \in N(i)$ and some

path set $P_{x_0, \tilde{j}}^i \subset \mathbb{P}_{x_0, \tilde{j}}$. As the travel time is nonnegative on every edge by (2.10), the travel time is monotone over increasing path length and we have $T(p_{x_0, i_{k-1}}) < T(p_{x_0, j})$ with $i_{k-1}, j \in N(i)$, implying that $p_{x_0, j}$ with $i \in p_{x_0, j}$ cannot be a minimiser. Hence, we write

$$\begin{aligned} u_i &= \min_{x_0 \in \partial V} \min_{j \in N(i)} \min_{P_{x_0, j} \subset \mathbb{P}_{x_0, j}} \left(T(P_{x_0, j}) + \frac{s_i}{w_{j, i}} \right) \\ &= \min_{j \in N(i)} \left(\left(\min_{x_0 \in \partial V} \min_{P_{x_0, j}^i \subset \mathbb{P}_{x_0, j}} T(P_{x_0, j}) \right) + \frac{s_i}{w_{j, i}} \right) \\ &= \min_{j \in N(i)} \left(u_j + \frac{s_i}{w_{j, i}} \right). \end{aligned}$$

We move u_i to the right hand side, and use that $\min(x) = -\max(-x)$, so that we obtain

$$0 = \max_{j \in N(i)} \left(u_i - u_j - \frac{s_i}{w_{j, i}} \right) = \max_{j \in N(i)} \left(\frac{w_{j, i} (u_i - u_j) - s_i}{w_{j, i}} \right).$$

Due to the positivity of w_{ij} , this is equivalent to $\max_{j \in N(i)} (w_{j, i} (u_i - u_j) - s_i) = 0$, and as $u_i \geq u_j$, this yields

$$\max_{j \in N(i)} (w_{j, i} (u_i - u_j)^+) = s_i,$$

that is, we obtain model 3($p = \infty$) in (2.16).

3.2.2. Equivalence between Models 2(ii) and 3($p = 2$). Starting with (2.5) and considering travel time of model 2(ii) in (2.7) yields

$$\begin{aligned} u_i &= \min_{x_0 \in \partial V} \min_{P_{x_0, i} \subset \mathbb{P}_{x_0, i}} T(P_{x_0, i}) \\ &= \min_{x_0 \in \partial V} \min_{P_{x_0, i} \subset \mathbb{P}_{x_0, i}} \left(\frac{1}{z_{x_0, i}} \sum_{j \in K(P_{x_0, i})} w_{j, i}^2 T(P_{x_0, j}^i) \right. \\ &\quad \left. + \frac{1}{z_{x_0, i}} \sqrt{\left(\sum_{j \in K(P_{x_0, i})} w_{j, i}^2 T(P_{x_0, j}^i) \right)^2 + z_{x_0, i} s_i^2 - z_{x_0, i} \sum_{j \in K(P_{x_0, i})} w_{j, i}^2 (T(P_{x_0, j}^i))^2} \right) \end{aligned}$$

where

$$z_{x_0, i} = \sum_{j \in K(P_{x_0, i})} w_{j, i}^2.$$

We can write u_i as

$$\begin{aligned} u_i &= \min_{x_0 \in \partial V} \min_{K \subset N(i)} \min_{\{P_{x_0, i} \subset \mathbb{P}_{x_0, i} : K(P_{x_0, i}) = K\}} \left(\frac{1}{z_K} \sum_{j \in K} w_{j, i}^2 T(P_{x_0, j}^i) \right. \\ &\quad \left. + \frac{1}{z_K} \sqrt{\left(\sum_{j \in K} w_{j, i}^2 T(P_{x_0, j}^i) \right)^2 + z_K s_i^2 - z_K \sum_{j \in K} w_{j, i}^2 (T(P_{x_0, j}^i))^2} \right), \end{aligned}$$

where

$$z_K = \sum_{j \in K} w_{j, i}^2.$$

Since $T(P_{x_0, j}^i)$ is the only term depending on $x_0 \in \partial V$ and $P_{x_0, j}^i$ satisfying $P_{x_0, i} = (P_{x_0, j}^i, (j, i)) \subset \mathbb{P}_{x_0, i}$ with $j \in K(P_{x_0, i})$, we may pull the minimisation with respect to these parameters inside

the expression, and replace the minimisation with respect to $P_{x_0,i} = (P_{x_0,j}^i, (j,i)) \subset \mathbb{P}_{x_0,i}$ with $j \in K(P_{x_0,i})$ by $P_{x_0,j} \subset \mathbb{P}_{x_0,j}$ as in Section 3.2.1. This yields

$$u_i = \min_{K \subset N(i)} \left(\frac{1}{z_K} \sum_{j \in K} w_{j,i}^2 u_j + \frac{1}{z_K} \sqrt{\left(\sum_{j \in K} w_{j,i}^2 u_j \right)^2 + z_K s_i^2 - z_K \sum_{j \in K} w_{j,i}^2 u_j^2} \right)$$

where

$$u_j = \min_{x_0 \in \partial V} \min_{P_{x_0,j} \subset \mathbb{P}_{x_0,j}} T(P_{x_0,j})$$

by definition. Moving u_i to the right-hand-side and using $\min(x) = -\max(-x)$ provides

$$0 = \max_{K \subset N(i)} \left(\frac{1}{z_K} \sum_{j \in K} w_{j,i}^2 (u_i - u_j) - \frac{1}{z_K} \sqrt{\left(\sum_{j \in K} w_{j,i}^2 u_j \right)^2 + z_K s_i^2 - z_K \sum_{j \in K} w_{j,i}^2 u_j^2} \right).$$

To achieve that the expression vanishes, we require that the first term is nonnegative which is equivalent to $K \subset N(i)$ such that $u_j \leq u_i$ for all $j \in K$. Note that the first term is maximal for the set $\{j \in N(i) : u_j \leq u_i\}$ and the magnitude of the second term decreases as the size of the set K increases. Hence, the maximiser K with $K = \{j \in N(i) : u_j \leq u_i\}$ satisfies

$$z_K u_i - \sum_{j \in K} w_{j,i}^2 u_j = \sqrt{\left(\sum_{j \in K} w_{j,i}^2 u_j \right)^2 + z_K s_i^2 - z_K \sum_{j \in K} w_{j,i}^2 u_j^2}.$$

Squaring both sides and dividing by z_K yields

$$z_K u_i^2 - 2u_i \sum_{j \in K} w_{j,i}^2 u_j = s_i^2 - \sum_{j \in K} w_{j,i}^2 u_j^2,$$

i.e.

$$s_i^2 = \sum_{j \in K} w_{j,i}^2 (u_i - u_j)^2 = \sum_{j \in N(i) : u_j \leq u_i} w_{j,i}^2 (u_i - u_j)^2 = \sum_{j \in N(i)} w_{j,i}^2 ((u_i - u_j)^+)^2,$$

that is model 3($p = 2$) in (2.15).

3.2.3. Equivalence between Models 2(iii) and 3($p = 1$). We begin by using the first arrival model (2.5) with travel time T given as in model 2(iii) by (2.8) which yields

$$\begin{aligned} u_i &= \min_{x_0 \in \partial V} \min_{P_{x_0,i} \subset \mathbb{P}_{x_0,i}} T(P_{x_0,i}) \\ &= \min_{x_0 \in \partial V} \min_{P_{x_0,i} \subset \mathbb{P}_{x_0,i}} \frac{1}{\sum_{j \in K(P_{x_0,i})} w_{j,i}} \left(\sum_{j \in K(P_{x_0,i})} w_{j,i} T(P_{x_0,j}^i) + s_i \right) \\ &= \min_{K \subset N(i)} \min_{x_0 \in \partial V} \min_{\{P_{x_0,i} \subset \mathbb{P}_{x_0,i} : K(P_{x_0,i}) = K\}} \frac{1}{\sum_{j \in K} w_{j,i}} \left(\sum_{j \in K} w_{j,i} T(P_{x_0,j}^i) + s_i \right) \\ &= \min_{K \subset N(i)} \frac{1}{\sum_{j \in K} w_{j,i}} \left(\sum_{j \in K} w_{j,i} \min_{x_0 \in \partial V} \min_{P_{x_0,j} \subset \mathbb{P}_{x_0,j}} T(P_{x_0,j}) + s_i \right) \\ &= \min_{K \subset N(i)} \frac{1}{\sum_{j \in K} w_{j,i}} \left(\sum_{j \in K} w_{j,i} u_j + s_i \right), \end{aligned}$$

where we can use a similar argument as in Section 3.2.1 in the fourth equality to consider the sets $P_{x_0,j} \subset \mathbb{P}_{x_0,j}$ instead of the sets $P_{x_0,i} = (P_{x_0,j}^i, (j,i)) \subset \mathbb{P}_{x_0,i}$ with $j \in K(P_{x_0,i})$. Then we rearrange the equation resulting in

$$\min_{K \subset N(i)} \frac{1}{\sum_{j \in K} w_{j,i}} \left(\sum_{j \in K} w_{j,i} (u_j - u_i) + s_i \right) = 0,$$

and as $\sum_{j \in K} w_{j,i} > 0$, we obtain

$$s_i = - \min_{K \subset N(i)} \left(\sum_{j \in K} w_{j,i} (u_j - u_i) \right) = \max_{K \subset N(i)} \sum_{j \in K} w_{j,i} (u_i - u_j).$$

If $u_j \leq u_i$ then the summand is positive and therefore the maximizer over $K \subset N(i)$ is the set $\{j \in N(i) : u_j \leq u_i\}$. Hence we arrive at

$$s_i = \sum_{j \in N(i) : u_j \leq u_i} w_{j,i} (u_i - u_j) = \sum_{j \in N(i)} w_{j,i} (u_i - u_j)^+,$$

that is, model 3($p = 1$) in (2.15).

4. FORMAL EIKONAL CONTINUUM LIMIT ON THE EUCLIDEAN PLANE

Since we are interested in very large numbers n of data points, it can be convenient to consider the associated mean-field equations instead of large discrete systems. In this section, we assume that the data points are associated with points in the Euclidean plane so that $V = \{X_1, \dots, X_n\}$ where each $X_i \in \mathbb{R}^2$.

4.1. General setting. To formulate the limit $n \rightarrow \infty$, we assume that the data points $V = \{X_1, \dots, X_n\}$ in the Euclidean plane \mathbb{R}^d , $d \geq 1$, are samples from a probability measure $\rho \in \mathcal{P}(\Omega)$ where $\mathcal{P}(\Omega)$ denotes the space of probability measures on $\Omega \subset \mathbb{R}^d$. Given $X_1, \dots, X_n \in \mathbb{R}^d$ distributed as ρ , we consider the associated empirical measure $\rho_n(x) = \frac{1}{n} \sum_{i=1}^n \delta_{X_i}(x)$.

To connect the discrete space \mathcal{H}^n on V with functions on Ω , we consider continuous interpolations. For $v \in \mathcal{H}^n$, we introduce the function $V^n: \Omega \rightarrow \mathbb{R}$ satisfying $V^n \in C(\Omega)$, $V(X_i) = v(X_i) = v_i$ for all $i = 1, \dots, n$. For $s \in \mathcal{H}^n$ and $u \in \mathcal{H}^n$, we consider $S^n, U^n \in C(\Omega)$ with $S^n(X_i) = s(X_i) = s_i$ and $U^n(X_i) = u(X_i) = u_i$, respectively. This results in a sequence of graphs with n vertices with slowness functions S^n and arrival times U^n where we suppose that the point-wise limits as $n \rightarrow \infty$ exist and the point-wise limit functions are denoted by S and U , respectively. We replace the discrete weights w_{ij} by a weight function $\bar{\eta}: \mathbb{R}^2 \rightarrow [0, \infty)$. We assume that the kernel $\bar{\eta}$ is isotropic and given by the radial profile $\eta: [0, \infty) \rightarrow [0, \infty)$, i.e. $\bar{\eta}(x) = \eta(\|x\|_2)$ for the 2-norm $\|\cdot\|_2$ in \mathbb{R}^d , satisfying

- (1) $\eta(0) > 0$ and η is continuous at 0.
- (2) η is non-increasing.
- (3) $\bar{B}_1(0) \subset \text{supp } \eta$.

Note that the assumptions on η are not restrictive and include a broad class of kernels.

Since all nodes of the graph are assumed to be in Euclidean space, we assign the weight

$$w_{ij} = \eta(\|X_i - X_j\|_2) \quad (4.1)$$

on edge (i, j) for node i and its neighbour $j \in N(i)$ of the finite graph. We assume that $\|X_i - X_j\|_2 \rightarrow 0$ uniformly as $n \rightarrow \infty$. For any $n \in \mathbb{N}$ we introduce a parameter $\varepsilon = \varepsilon(n)$. We suppose that $\varepsilon \sim \max_{i \in V} \max_{j \in N(i)} \|X_i - X_j\|_2$ as $n \rightarrow \infty$, i.e. $\varepsilon \rightarrow 0$ as $n \rightarrow \infty$. To take the data density into account, we rescale η appropriately as the number n of data points increases. This can be achieved by considering $\eta_\varepsilon: [0, \infty) \rightarrow [0, \infty)$, $\eta_\varepsilon = \eta(\frac{\cdot}{\varepsilon})$. The scaling by ε implies that the support of η is scaled by ε .

We formulate the discrete eikonal equations (2.14) in the notation introduced above for $1 \leq p \leq \infty$. Using the definition of w_{ij} in (4.1) and rescaling by ε we obtain

$$\frac{1}{\varepsilon^p} \sum_{j \in N(i)} (\eta_\varepsilon(\|X_i - X_j\|_2) (U^n(X_i) - U^n(X_j))^+)^p = S^n(X_i)^p, \quad i \in V,$$

$$U^n(X_i) = 0, \quad i \in \partial V,$$

for $1 \leq p < \infty$. Under appropriate smoothness assumptions on the continuous interpolant U^n and for $\|X_j - X_i\|_2$ sufficiently small, we have $U^n(X_j) = U^n(X_i) + \nabla U^n(X_i) \cdot (X_j - X_i) + \mathcal{O}(\|X_j - X_i\|_2^2)$ for $j \in N(i)$. For $i \in V$, this yields

$$\begin{aligned} S^n(X_i)^p &= \sum_{j \in N(i)} \eta_\varepsilon(\|X_i - X_j\|_2)^p \left(\left(\frac{U^n(X_i) - U^n(X_j)}{\varepsilon} \right)^+ \right)^p \\ &= \sum_{j \in N(i)} \eta_\varepsilon(\|X_i - X_j\|_2)^p \left(\left(\nabla U^n(X_i) \cdot \frac{X_i - X_j}{\varepsilon} \right)^+ \right)^p + \mathcal{O} \left(\frac{\|X_i - X_j\|_2^{2p}}{\varepsilon^p} \right), \end{aligned}$$

provided n is sufficiently large and hence $\|X_i - X_j\|_2$ is sufficiently small. For $\varepsilon \sim \max_{i \in V} \max_{j \in N(i)} \|X_i - X_j\|_2$ as $n \rightarrow \infty$ and $1 \leq p < \infty$, this suggests to seek a sufficiently smooth function satisfying

$$\sum_{j \in N(i)} \eta_\varepsilon(\|X_i - X_j\|_2)^p \left(\left(\nabla U^n(X_i) \cdot \frac{X_i - X_j}{\varepsilon} \right)^+ \right)^p = S^n(X_i)^p \quad (4.2)$$

at each vertex i .

In the case $p = \infty$, we consider (2.16) with weights w_{ij} in (4.1) and rescale by ε to obtain

$$\frac{1}{\varepsilon} \max_{j \in N(i)} \{ \eta_\varepsilon(\|X_i - X_j\|_2) (U^n(X_i) - U^n(X_j))^+ \} = S^n(X_i), \quad i \in V,$$

$$U^n(X_i) = 0, \quad i \in \partial V.$$

It follows that

$$\begin{aligned} S^n(X_i) &= \max_{j \in N(i)} \left\{ \eta_\varepsilon(\|X_i - X_j\|_2) \left(\frac{U^n(X_i) - U^n(X_j)}{\varepsilon} \right)^+ \right\} \\ &= \max_{j \in N(i)} \left\{ \eta_\varepsilon(\|X_i - X_j\|_2) \left(\nabla U^n(X_i) \cdot \frac{X_i - X_j}{\varepsilon} \right)^+ \right\} + \mathcal{O} \left(\frac{\|X_i - X_j\|_2^2}{\varepsilon} \right) \end{aligned}$$

for $i \in V$. Hence, we obtain the model

$$\max_{j \in N(i)} \left\{ \eta_\varepsilon(\|X_i - X_j\|_2) \left(\nabla U^n(X_i) \cdot \frac{X_i - X_j}{\varepsilon} \right)^+ \right\} = S^n(X_i) \quad (4.3)$$

for $i \in V$.

4.1.1. Regular graphs. The form of the model in (4.2) for any $1 \leq p < \infty$ and (4.3) for $p = \infty$ motivates the consideration of regular grids for which the dependence on $N(i)$ simplifies. In this section, we consider regular grids in Euclidean space as graphs where we suppose that every node of the grid has κ neighbors. Examples of grids in the plane, $d = 2$, are given by hexagonal grids ($\kappa = 3$), square grids ($\kappa = 4$) and triangular grids ($\kappa = 6$ and $\kappa = 8$). A special instance is also the regular one-dimensional grid with $\kappa = 2$. Examples of regular κ -neighbor grids with equal grid lengths are shown in Figure 4 for $\kappa \in \{2, 3, 4, 6\}$, while examples of regular κ -neighbor grids with different grid lengths in each direction are shown in Figure 5 for $\kappa \in \{4, 6\}$.

4.2. Formal limit for specific regular grids for any p . In this section, we discuss the formal limit as $n \rightarrow \infty$ for specific regular grids for any p . We identify \mathbb{R}^2 with \mathbb{C} and consider the vectors $\tilde{\xi}_j = r_j \exp(2\pi i j / \kappa)$ with $r_j \in (0, 1]$ for $j = 1, \dots, \kappa$. For a fixed ϕ , we denote the rotation matrix of angle $\phi \in \mathbb{R}$ by

$$R_\phi = \begin{pmatrix} \cos \phi & -\sin \phi \\ \sin \phi & \cos \phi \end{pmatrix}.$$

For a given grid defined by $\tilde{\xi}_j, j = 1, 2, \dots, \kappa$ we may rotate by ϕ and set $\xi_j = R_\phi \tilde{\xi}_j$.

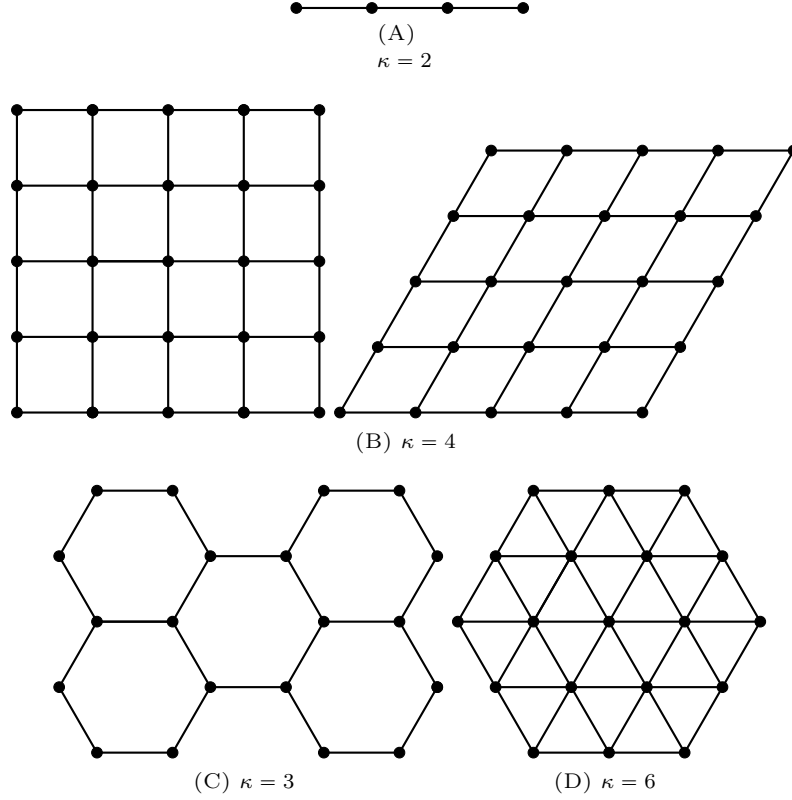
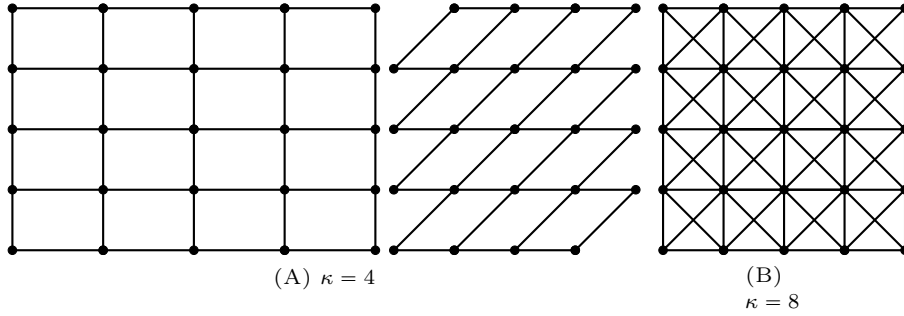
To guarantee $\varepsilon \sim \max_{i \in V} \max_{j \in N(i)} \|X_i - X_j\|_2$ as $n \rightarrow \infty$, we scale the direction vectors ξ_j by ε and for any $i \in V$ and $j \in N(i)$ we obtain $X_j = X_i + \varepsilon \xi_k$ for some $k \in \{1, \dots, \kappa\}$. Since $\xi_k \in \text{supp } \eta$ and $k \in \{1, \dots, \kappa\}$ by Assumption (3), this implies that $\varepsilon \xi_k = (X_i + \varepsilon \xi_k) - X_i \in \text{supp } \eta_\varepsilon$. For $i \in V$, (4.2) and (4.3) reduce to

$$\sum_{j=1}^{\kappa} \eta(\|\xi_j\|_2)^p \left((\nabla U^n(X_i) \cdot \xi_j)^+ \right)^p = S^n(X_i)^p \quad (4.4)$$

for any $1 \leq p < \infty$, and

$$\max_{j \in \{1, \dots, \kappa\}} \left\{ \eta(\|\xi_j\|_2) (\nabla U^n(X_i) \cdot \xi_j)^+ \right\} = S^n(X_i), \quad (4.5)$$

respectively.

FIGURE 4. Illustration of regular κ -neighbor grids with equal grid lengths.FIGURE 5. Illustration of regular κ -neighbor grids with different grid lengths.

4.2.1. Triangular grid, $d = 2$. For the two-dimensional triangular grid, we consider

$$\xi_1 = (1, 0), \quad \xi_2 = (\cos(\pi/3), \sin(\pi/3)) \quad \text{and} \quad \xi_3 = (\cos(2\pi/3), \sin(2\pi/3)). \quad (4.6)$$

At each grid point $i \in V$, we have 6 grid directions ζ_k for $k = 1, \dots, 6$ with $\zeta_k = \xi_k$ and $\zeta_{k+3} = -\xi_k$ for $k = 1, 2, 3$. Note that any other 2-dimensional triangular grid can be studied in a similar way by rotating ξ_1, ξ_2, ξ_3 by some angle $\phi \in \mathbb{R}$. In the formal limit $n \rightarrow \infty$, we obtain

$$\sum_{k=1}^3 |\nabla U(x) \cdot \xi_k|^p = (S(x)/\eta(1))^p, \quad x \in \Omega, \quad (4.7)$$

for $1 \leq p < \infty$ and

$$\max_{k=1,2,3} |\nabla U(x) \cdot \xi_k| = S(x)/\eta(1), \quad x \in \Omega, \quad (4.8)$$

for $p = \infty$, subject to appropriate boundary conditions. Note that (4.7) and (4.8) can be summarised as

$$\|(\nabla U(x) \cdot \xi_k)_{k=1,2,3}\|_p = S(x)/\eta(1), \quad x \in \Omega, \quad (4.9)$$

for any $1 \leq p \leq \infty$. For $p = 2$, (4.9) reduces to

$$\|\nabla U(x)\|_2 = \frac{\sqrt{2}}{\sqrt{3}} S(x)/\eta(1), \quad x \in \Omega,$$

since $\xi_1 = e_1$, $\xi_2 = \frac{1}{2}e_1 + \frac{\sqrt{3}}{2}e_2$ and $e_3 = -\frac{1}{2}e_1 + \frac{\sqrt{3}}{2}e_2$.

In the following, we show examples of nonnegative, Lipschitz continuous functions which satisfy the equation (4.9) almost everywhere for different choices of p and the specific case when $S = 1$.

Remark 4.1 (Solutions for $S = 1$ and $p = \infty$). For $S = 1$ and $p = \infty$, we show that the nonnegative, Lipschitz continuous function $U(x) = \frac{1}{\eta(1)} \max_{k=1,2,3} |x \cdot \xi_k|$ satisfies (4.9) with $U(0) = 0$. Suppose that for x given, l is chosen so that $U(x) = \frac{1}{\eta(1)} |x \cdot \xi_l|$. Then, $\nabla U(x) = \frac{1}{\eta(1)} \frac{x \cdot \xi_l}{|x \cdot \xi_l|} \xi_l$ and hence

$$\eta(1) \max_{k=1,2,3} \left| \frac{1}{\eta(1)} \frac{x \cdot \xi_l}{|x \cdot \xi_l|} \xi_l \cdot \xi_k \right| = \max_{k=1,2,3} |\xi_l \cdot \xi_k| = 1.$$

Note that the functions $U_l(x) = \frac{1}{\eta(1)} |x \cdot \xi_l|$ for $l \in \{1, 2, 3\}$ satisfy $\nabla U_l(x) = \frac{1}{\eta(1)} \frac{x \cdot \xi_l}{|x \cdot \xi_l|} \xi_l$ and hence U_l for $l \in \{1, 2, 3\}$ are solutions to (4.9) for $p = \infty$. Next, we rotate the above solution U by $\pi/6$ and rescale the solution appropriately, resulting in $\tilde{U}(x) = \frac{1}{\eta(1) \cos(\pi/6)} \max_{k=1,2,3} |x \cdot R_{\pi/6} \xi_k|$. One can show that \tilde{U} is also a solution to (4.9) for $p = \infty$ with $\tilde{U}(0) = 0$. Note that \tilde{U} is also observed in the numerical experiments for the triangular grid in Figure 7. Similarly as above, one can also show that $\tilde{U}_l(x) = \frac{1}{\eta(1) \cos(\pi/6)} |x \cdot R_{\pi/6} \xi_l|$ for $l \in \{1, 2, 3\}$ satisfies (4.9).

Remark 4.2 (Solutions for $S = 1$ and $p = 2$). For $S = 1$ and $p = 2$, clearly $U(x) = \frac{\sqrt{2}}{\sqrt{3}} \|x\|_2$ is a Lipschitz continuous function satisfying the mean field equation (4.9) and $U(0) = 0$. Note that $U(x) = \frac{\sqrt{2}}{\sqrt{3}\eta(1)} \|x\|_2$ is also observed in the numerical simulations in Figure 7.

Remark 4.3 (Solutions for $S = 1$ and $p = 1$). Focussing on $S = 1$ and $p = 1$, we consider $U(x) = \frac{1}{2\eta(1)} \max_{k=1,2,3} |x \cdot \xi_k|$. For x given, suppose that l is chosen so that $U(x) = \frac{1}{2\eta(1)} |x \cdot \xi_l|$. Then, $\nabla U(x) = \frac{1}{2\eta(1)} \frac{x \cdot \xi_l}{|x \cdot \xi_l|} \xi_l$ and hence

$$\eta(1) \sum_{k=1}^3 |\nabla U(x) \cdot \xi_k| = \frac{1}{2} \sum_{k=1}^3 |\xi_l \cdot \xi_k| = \frac{1}{2} (1 + 2 \cos(\pi/3)) = 1.$$

Thus we have a nonnegative, Lipschitz continuous solution of the mean field equation (4.9) that vanishes at 0. Note that scaling this function by 2 yields one of the solution when $p = \infty$ and $S = 1$. In addition to this solution, we can consider a rotation by $\pi/6$ with appropriate scaling of the form $\tilde{U}(x) = \frac{1}{2\eta(1) \cos(\pi/6)} \max_{k=1,2,3} |x \cdot R_{\pi/6} \xi_k|$. For x given, suppose that l is chosen so that $\tilde{U}(x) = \frac{1}{2\eta(1) \cos(\pi/6)} |x \cdot R_{\pi/6} \xi_l|$. Then, $\nabla \tilde{U}(x) = \frac{1}{2\eta(1) \cos(\pi/6)} \frac{x \cdot R_{\pi/6} \xi_l}{|x \cdot R_{\pi/6} \xi_l|} R_{\pi/6} \xi_l$ and hence

$$\eta(1) \sum_{k=1}^3 |\nabla \tilde{U}(x) \cdot \xi_k| = \frac{1}{2 \cos(\pi/6)} \sum_{k=1}^3 |R_{\pi/6} \xi_l \cdot \xi_k| = 1.$$

The solution $\tilde{U}(x)$ is also observed in the numerical experiments in Figure 7 and scaling by 2 yields one of the solutions for $S = 1$ and $p = \infty$ in Remark 4.1.

4.2.2. d -dimensional parallelotopes. For a regular grid of parallelotopes in the d -dimensional Euclidean space, e.g. $\kappa = 2$ or $\kappa = 4$ in Figure 4 and $\kappa = 4$ in Figure 5, it is easy to see that $\kappa = 2d$. The grid directions at each node $i \in V$ are identical for parallelotopes which allows us to replace given ξ_1, \dots, ξ_κ by $R_\phi^{-1}\xi_1, \dots, R_\phi^{-1}\xi_\kappa$. and obtain equivalent equations. For the special case of the square grid, we have $\xi_k = e_k$ for $k = 1, \dots, d$ where e_k denotes the standard orthonormal basis in d dimensions.

We can order ξ_1, \dots, ξ_κ in such a way that $\xi_{d+1} = -\xi_1, \dots, \xi_{2d} = -\xi_d$. From (4.4) and (4.5), we obtain

$$\begin{aligned} & \sum_{k=1}^d \eta(\|\xi_k\|_2)^p |\nabla U^n(X_i) \cdot \xi_k|^p \\ &= \sum_{k=1}^d \eta(\|\xi_k\|_2)^p ((-\nabla U^n(X_i) \cdot \xi_k)^+)^p + \sum_{k=1}^d \eta(\|\xi_k\|_2)^p ((\nabla U^n(X_i) \cdot \xi_k)^+)^p \\ &= \sum_{j \in N(i)} \eta(\|\xi_j\|_2)^p ((\nabla U^n(X_i) \cdot \xi_j)^+)^p = S^n(X_i)^p \end{aligned}$$

for $i \in V$ and $1 \leq p < \infty$, and

$$\begin{aligned} \max_{k=1, \dots, d} \{\eta(\|\xi_k\|_2) |\nabla U^n(X_i) \cdot \xi_k|\} &= \max_{k=1, \dots, d} \{\eta(\|\xi_k\|_2) (\mp \nabla U^n(X_i) \cdot \xi_k)^+\} \\ &= \max_{j \in N(i)} \{\eta(\|\xi_j\|_2) (\nabla U^n(X_i) \cdot \xi_j)^+\} = S^n(X_i) \end{aligned}$$

for $i \in V$ and $p = \infty$, respectively. Since the direction vectors ξ_k for $k = 1, \dots, d$ are independent of any $i \in V$ and assuming that ∇U and S are continuous, the formal limits as $n \rightarrow \infty$ reads

$$\sum_{k=1}^d \eta(\|\xi_k\|_2)^p |\nabla U(x) \cdot \xi_k|^p = S(x)^p, \quad x \in \Omega,$$

for $1 \leq p < \infty$, and

$$\max_{k=1, \dots, d} \{\eta(\|\xi_k\|_2) |\nabla U(x) \cdot \xi_k|\} = S(x), \quad x \in \Omega,$$

for $p = \infty$, respectively, with appropriate boundary conditions. These may be rewritten, for each $p \in [1, \infty]$, as

$$\|A \nabla U(x)\|_p = S(x) \quad x \in \Omega,$$

where $A \in \mathbb{R}^{d \times d}$ has rows

$$\text{Row}_k(A) = \eta(\|\xi_k\|_2) \xi_k^T, \quad k = 1, \dots, d.$$

For parallelotopes of equal grid lengths as shown for $\kappa = 2$ or $\kappa = 4$ in Figure 4, we have $\|\xi_j\|_2 = r_j = 1$ for all $j = 1, \dots, d$, implying that

$$\text{Row}_k(A) = \eta(1) \xi_k^T, \quad k = 1, \dots, d.$$

Thus, the formal limit reduces to

$$\|\nabla U(x)\|_p = S(x)/\eta(1), \quad x \in \Omega. \quad (4.10)$$

Remark 4.4 (Solutions for $S = 1$ and any $1 \leq p \leq \infty$). We focus on $S = 1$, $\eta(1) = 1$ and $\xi_k = e_k, k = 1, 2, \dots, d$. We show that the q -norm $\|\cdot\|_q$ where q such that $\frac{1}{p} + \frac{1}{q} = 1$ is a solution to (4.10). This generalises the fact that the Euclidean distance is the viscosity solution of Euclidean-norm eikonal equation with slowness 1. For $1 \leq q < \infty$, we have $\|\nabla \|x\|_q\|_p = \|x\|_q^{1-q} (|x_k|^{q-2} x_k)_{k=1}^d$ (where $x_k \neq 0$ for all $k = 1, \dots, d$), implying that

$$\|(\nabla \|x\|_q)\|_p = \|x\|_q^{1-q} (\|x\|_q^{q-1})_p,$$

for any $1 < p \leq \infty$. If q satisfies $\frac{1}{p} + \frac{1}{q} = 1$ in addition, we obtain

$$\|x\|_q^{q-1} = \left(\sum_{k=1}^d |x_k|^{(q-1)p} \right)^{\frac{1}{p}} = \left(\sum_{k=1}^d |x_k|^q \right)^{\frac{q-1}{q}} = \|x\|_q^{q-1},$$

which yields $\|(\nabla\|x\|_q)\|_p = 1$. We conclude that for $1 < p \leq \infty$, there exists $1 \leq q < \infty$ with $\frac{1}{p} + \frac{1}{q} = 1$ such that $U(x) = \|x\|_q$ is a solution to (4.10).

To determine $\nabla\|x\|_q$ for $q = \infty$, we choose $l \in \{1, \dots, d\}$ such that $|x_l| = \|x\|_q$. Then, $\nabla\|x\|_q = \frac{x_l}{|x_l|}e_l$, implying that $\|\nabla\|x\|_q\|_1 = 1$ and hence $U(x) = \|x\|_\infty$ is a solution to (4.10) for $p = 1$. This shows that for any $1 \leq p \leq \infty$, $U(x) = \|x\|_q$ is a solution to (4.10) where q satisfies $\frac{1}{p} + \frac{1}{q} = 1$. For the one-dimensional setting, i.e. $d = 1$, the unique solution to (4.10) is given by $U(x) = |x|$ for any $1 \leq p \leq \infty$. For higher dimensions, examples include $(p, q) = (2, 2)$ with solution $U(x) = \|x\|_2$, $(p, q) = (\infty, 1)$ with solution $U(x) = \|x\|_1$ and $(p, q) = (1, \infty)$ with solution $U(x) = \|x\|_\infty$. These solutions can also be observed in the numerical experiments in Figure 7 in Section 5. Note that for $p = \infty$, another solution is given by $U(x) = \|x\|_\infty$ which is not observed in the numerical simulations in Figure 7.

4.2.3. Hexagonal planar grid. In this section, we consider a hexagonal grid in the Euclidean plane with ξ_1, ξ_2 and ξ_3 as in (4.6). Note that any rotation of a hexagonal grid in the Euclidean plane can be studied in a similar way by rotating ξ_1, ξ_2, ξ_3 by some angle $\phi \in \mathbb{R}$. At each grid point $i \in V$, we either have the grid directions $\zeta_k = (-1)^k \xi_k$ for $k = 1, 2, 3$ or $\zeta_k = (-1)^{k+1} \xi_k$ for $k = 1, 2, 3$. Further, all grid lengths are equal, implying that we may assume that $\|\xi_j\|_2 = r_j = 1$ for all $j = 1, 2, 3$. For any $i \in V$, we have

$$\eta(1)^p \sum_{k=1}^3 ((\nabla U^n(X_i) \cdot \zeta_k)^+)^p = S^n(X_i)^p$$

for $1 \leq p < \infty$ by (4.4) and

$$\eta(1) \max_{k=1,2,3} \{(\nabla U^n(X_i) \cdot \zeta_k)^+\} = S^n(X_i)$$

for $p = \infty$ by (4.5). For any $i \in V$ with grid directions $\zeta_k = (-1)^k \xi_k$ for $k = 1, 2, 3$, we have

$$\eta(1)^p \sum_{k=1}^3 (((-1)^k \nabla U^n(X_i) \cdot \xi_k)^+)^p = S^n(X_i)^p \quad (4.11)$$

for $1 \leq p < \infty$ and

$$\eta(1) \max_{k=1,2,3} \{((-1)^k \nabla U^n(X_i) \cdot \xi_k)^+\} = S^n(X_i) \quad (4.12)$$

for $p = \infty$. Any neighbour $j \in N(i)$ of i has grid directions $\zeta_k = (-1)^{k+1} \xi_k$ for $k = 1, 2, 3$ and we have

$$\eta(1)^p \sum_{k=1}^3 (((-1)^{k+1} \nabla U^n(X_j) \cdot \xi_k)^+)^p = S^n(X_j)^p$$

for $1 \leq p < \infty$ and

$$\eta(1) \max_{k=1,2,3} \{((-1)^{k+1} \nabla U^n(X_j) \cdot \xi_k)^+\} = S^n(X_j)$$

for $p = \infty$. It is not clear how to merge these alternating equations in order to obtain a mean field limit.

4.3. Formal limit for regular κ -neighbor grid for κ even and $p = 2$. In this section, we consider a regular grid in the two-dimensional setting where every node has κ neighbors for an even number κ . We show that the formal limit and its solution are independent of the underlying regular κ -neighbor grid for $p = 2$. From (4.4) with $p = 2$, we have that

$$\eta(1)^2 \sum_{j=1}^{\kappa} \left((\nabla U^n(X_i) \cdot (R_{\phi_i} \xi_j))^+ \right)^2 = S^n(X_i)^2$$

for $i \in V$. We only consider the positive part in the above sum, implying that, since κ is even, $\kappa/2$ summands are zero. We obtain

$$\eta(1)^2 \sum_{j=1}^{\kappa/2} |\nabla U^n(X_i) \cdot (R_{\phi_i} \xi_j)|^2 = S^n(X_i)^2.$$

Since $R_{\phi_i} \xi_j = \exp(i(\phi_i + 2\pi j/\kappa)) = \cos(\phi_i + 2\pi j/\kappa) + i \sin(\phi_i + 2\pi j/\kappa)$, we have

$$\begin{aligned} & \eta(1)^2 \sum_{j=1}^{\kappa/2} |\partial_1 U^n(X_i) \cos(\phi_i + 2\pi j/\kappa) + \partial_2 U^n(X_i) \sin(\phi_i + 2\pi j/\kappa)|^2 \\ &= \eta(1)^2 \sum_{j=1}^{\kappa/2} (\partial_1 U^n(X_i))^2 \cos^2(\phi_i + 2\pi j/\kappa) + (\partial_2 U^n(X_i))^2 \sin^2(\phi_i + 2\pi j/\kappa) = S^n(X_i)^2 \end{aligned}$$

where we used that

$$\sum_{j=1}^{\kappa/2} \cos(\phi_i + 2\pi j/\kappa) \sin(\phi_i + 2\pi j/\kappa) = \frac{1}{2} \sum_{j=1}^{\kappa/2} \sin 2(\phi_i + 2\pi j/\kappa) = 0.$$

By the properties of the geometric sum, we have

$$\sum_{j=1}^{\kappa/2} \exp^2(\phi_i + 2\pi j/\kappa) = 0$$

which implies that

$$\sum_{j=1}^{\kappa/2} \cos^2(\phi_i + 2\pi j/\kappa) = \sum_{j=1}^{\kappa/2} \sin^2(\phi_i + 2\pi j/\kappa) = \frac{\kappa}{4}.$$

We conclude that

$$\frac{\eta(1)^2 \kappa}{4} \|\nabla U^n(X_i)\|_2^2 = \frac{\eta(1)^2 \kappa}{4} \sum_{j=1}^2 |\partial_j U^n(X_i)|^2 = S^n(X_i)^2$$

for $i \in V$ and for the formal limit $n \rightarrow \infty$, we obtain

$$\frac{\eta(1)^2 \kappa}{4} \|\nabla U^n(X_i)\|_2^2 = S(x)^2, \quad x \in \Omega, \quad (4.13)$$

subject to appropriate boundary conditions. The continuum limits (4.13) for κ even are independent of the rotation matrix R_ϕ .

Remark 4.5. Specific examples for (4.13) for κ even include

$$\eta(1)^2 \|\nabla U^n(X_i)\|_2^2 = S(x)^2, \quad x \in \Omega,$$

for the square grid and

$$\frac{3\eta(1)^2}{2} \|\nabla U^n(X_i)\|_2^2 = S(x)^2, \quad x \in \Omega,$$

for the triangular grid. Hence, given the solution u on the square grid, the solution on the triangular grid is given by $\sqrt{4/6}u$ where the factor corresponds to the square root of the ratio between the number of neighbours for the square grid and the number of neighbours for the considered grid, i.e. six neighbours for the triangular grid.

4.4. Summary. In this section, we studied limiting PDEs of the discrete eikonal equation (4.4) and (4.5) for $1 \leq p < \infty$ and $p = \infty$, respectively, for different choices of the underlying grid. We set $S = 1$ and considered ξ_1, ξ_2, ξ_3 as in (4.6), i.e.

$$\xi_1 = (1, 0), \quad \xi_2 = (\cos(\pi/3), \sin(\pi/3)) \quad \text{and} \quad \xi_3 = (\cos(2\pi/3), \sin(2\pi/3)).$$

For any $1 \leq p \leq \infty$, the limiting PDE for the square grid is given by $\eta(1)\|\nabla U\|_p = S$, while for the triangular grid, we have $\eta(1)\|(\nabla U \cdot \xi_k)_{k=1,2,3}\|_p = S$. Hence, we may summarise the limiting PDE as $\|A\nabla U(x)\|_p = S(x)$ where $A = \eta(1)I_2 \in \mathbb{R}^{2 \times 2}$ with identity matrix $I_2 \in \mathbb{R}^{2 \times 2}$ for the square grid and $A \in \mathbb{R}^{3 \times 2}$ with rows $\text{Row}_k(A) = \eta(1)\xi_k^T$ for $k = 1, 2, 3$ for the triangular grid.

5. NUMERICAL EXAMPLES

5.1. Numerical methods. We solve discrete problems for each model by using front propagation. That is, we form the problems as in Section 2.1. This choice is motivated by the calculation numerical solutions to the eikonal equation on a square grid, which often uses front propagation; the discretization scheme is known as a fast marching method [21, 22]. Fast marching methods are efficient, and have an error analysis and proof of convergence to viscosity solutions of the eikonal equation [7]. They also produces adjoint solutions at no additional computational cost making it a useful approach in inverse problem settings [8].

5.2. Examples of models on specific grids. For each of our models, we solve a problem on a $[-1, 1] \times [-1, 1]$ domain. For interpretation and comparison with theory, we choose the simplest case where the slowness function $s(x) = 1$ everywhere, and we set the boundary condition $u_{(\cdot)}((0, 0)) = 0$. We solve for the discrete solution on four regular grids as shown in Figure 6, and denote the discrete solutions u_S, u_T, u_H, u_R for the square, triangular, hexagonal, and rhombus grids, respectively. All the regular grids have a fixed grid length h , and we set the constant weights $w_{i,j} = \frac{1}{h}$ for each edge of the grid (i, j) .

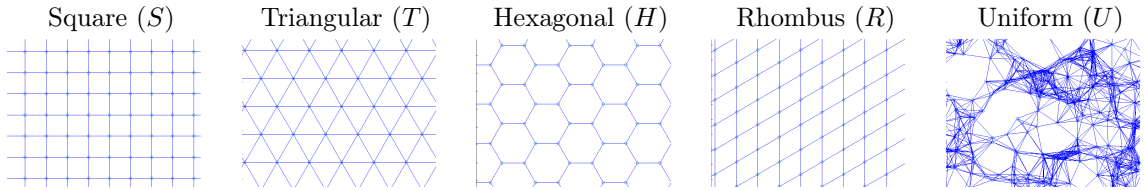


FIGURE 6. close-up views of the different graphs we use for the numerical results. The S, T, H , and R grids are regular, and we take a small interior angle of $\pi/3$, for the rhombus grid R . The U graph is created from connecting uniformly random points to nearest neighbours upto a cut-off radius 0.04 (leading to 12 average neighbours).

We present solutions of the discrete generalized eikonal equations $p = 1, \frac{3}{2}, 2, 3, \infty$ of which $p = 1, 2, \infty$ are contained in the theory of the previous sections, and $p = \frac{3}{2}, 3$ are natural extensions. The solutions for $h = 0.02$ are summarized in Figure 7. We see that all of the models depend on the underlying grid structure, however this is exhibited in different ways. Specifically for $p \neq 2$, we observed clear geometric dependency, as the discrete solution changes heterogeneously with the grid structure (the rows of Figure 7). For $p = 2$, we also see dependence on the mesh structure but this arises only through a constant factor (the colour scale of the $p = 2$ column in Figure 7). We also see a directional scaling in all solutions in the case of the rhombus grid, this is expected as when $s(x)$ constant, front propagation for square and rhombus grids are identical up to a linear transformation of the solution.

By taking these models on the specific grids, we indeed verify experimentally that the solutions in the cases $p = 1, 2, \infty$ coincide with solutions of the PDEs derived in Section 4 for the square and triangular grids.

We also look at a uniformly random ε -neighbour graph in the bounded domain as seen on the rightmost panel of Figure 6. This graph is produced by sampling M points from a uniform distribution over the domain, and define neighbours to be nodes within a distance $\varepsilon = 4/\sqrt{M}$ of each other. This choice leads experimentally to a well connected graph with an average of 12 neighbours per node. The average distance to any point in a disc radius ε to the centre is $1/\sqrt{2}\varepsilon$, therefore with our choice of ε , $M = 20000$ gives the average distance of h to any neighbour as 0.02. We now set $w_{i,j} = \frac{1}{\|i-j\|}$, and apply the front propagation algorithm. The results are displayed in Figure 8. We see that for any p we observe a rough radial symmetry, with solutions differing primarily due to a constant factor, and by an increasing smoothness in the solution level-lines as p increases.

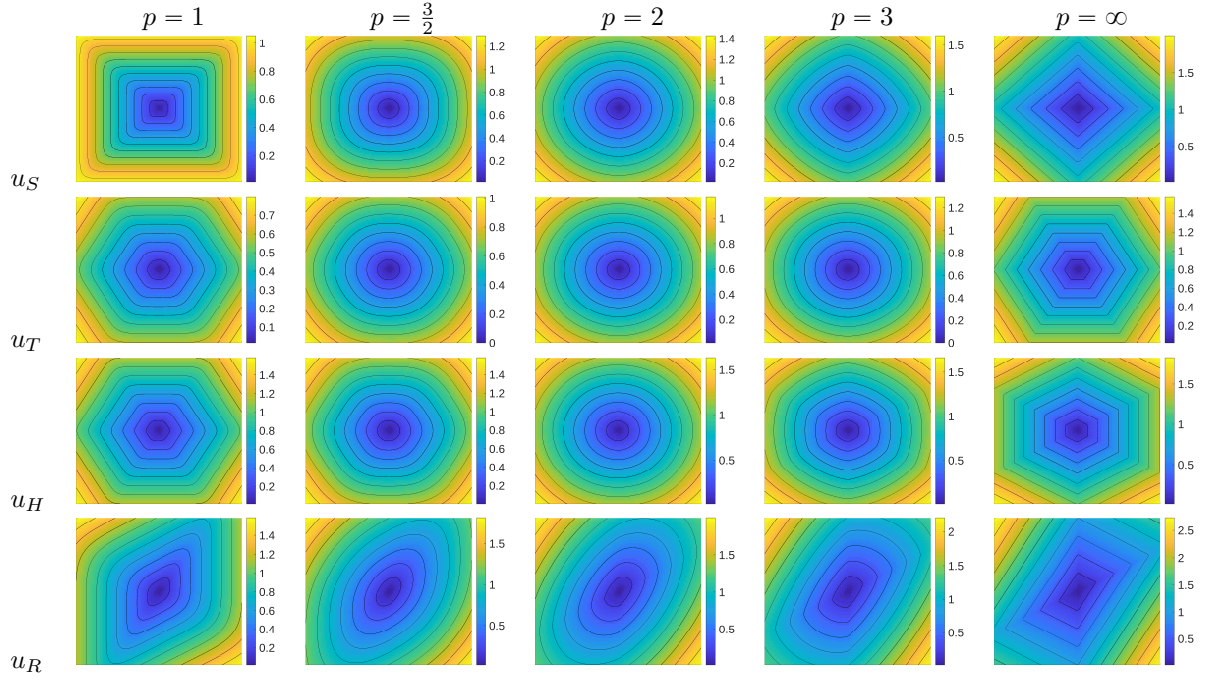


FIGURE 7. From top to bottom: the discrete solutions u_S on the square grid, u_T on the triangular grid, u_H on the hexagonal grid, u_R on the rhombus grid. From left to right: $p = 1, \frac{3}{2}, 2, 3, \infty$.

5.3. Validation of finite difference approximations for $p = 2$. From Section 5.2 it appears that we can hope to achieve an approximation to the Euclidean distance function on our domain as a solution for $s(x) = 1$ constant and $p = 2$ on the regular grids (S,T,H) and graph (U). Our setup is once again taken over a domain $[-1, 1] \times [-1, 1]$, and as shown in Figure 9 (left), we take a boundary condition fixed at (\circ) and observations at 10 random points (\times) in $[-1, 1] \times [-1, 1]$. We calculate the Euclidean distance (field shown in Figure 9 (right)) to these points, and we solve the fast marching problem for $p = 2$ and slowness $s(x) = 1$, for (S,T,H,U). For the grids we calculate the solutions u_S, u_T, u_H over mesh sizes $h = 0.08, 0.04, 0.02, 0.01$. For the uniform random graph, we do not choose h directly, instead we choose the sample size M so that the average distances between neighbours is approximately h ; we therefore choose $M = 1250, 5000, 20000, 80000$.

The Euclidean distance satisfies the limit PDE for the square grid almost everywhere, and so u_S is a valid finite difference approximation to the distance function. Using the formal analysis of Section 4.3 for $p = 2$, we can obtain the square solution by multiplying the solutions u_T by a constant scaling $c_T = \sqrt{3/4}$, and u_H by $c_H = \sqrt{6/4}$. We propose a related heuristic scaling for u_U ; we define $K = \text{mean}_i(|N(i)|)$ (average number of neighbours), and take $c_U = \sqrt{K/4}$. We then compare the solutions to the Euclidean distance between the source x_0 and observed points x_i in L^2 , multiplying the respective constant scalings c_* , and display the results in Table 2. In all cases we observe sublinear convergence in h to the Euclidean distance.

6. CONCLUSION

In this paper we proposed some models for information propagation on graphs. Underlying components of the models include a subset of nodes forming the initial source of information, the arrival times of information and the laws governing the transfer of information to nodes from their neighbours. The models are collected into three viewpoints. The first considers information moving as a wavefront across the graph from the sources and seeks the first hitting time of a front on any node. The wavefront always extends to the node with the smallest possible travel time and models calculate costs differently based on the current cost at neighbours within the wavefront.

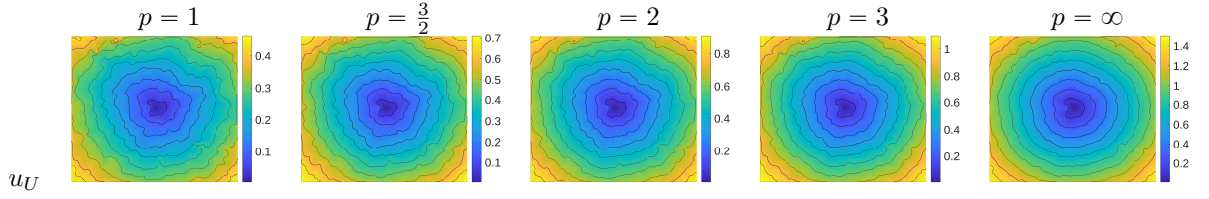


FIGURE 8. Discrete solution u_U for the uniformly random grid. From left to right: $p = 1, \frac{3}{2}, 2, 3, \infty$.

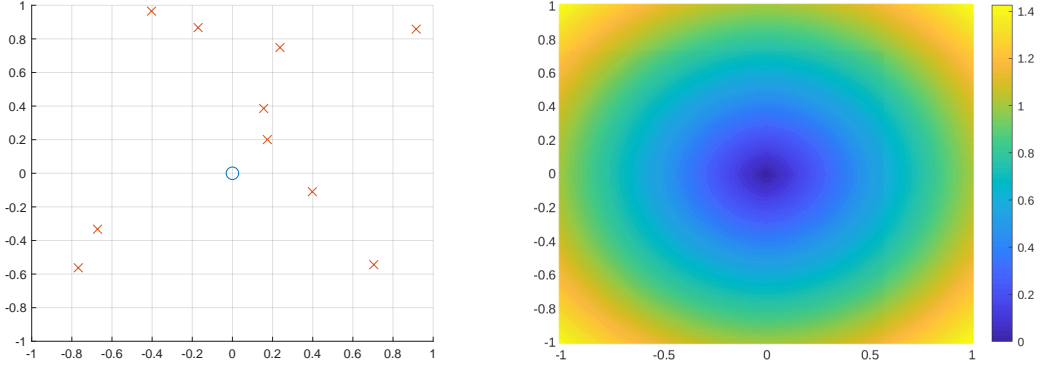


FIGURE 9. On the left we display the source (\circ) and 10 randomly chosen points $\{x_i\}$ (\times) where we compare our discrete solutions and the Euclidean distance. The Euclidean distance from the centre to any point in our domain is shown on the right.

h	$E_S(\{x_i\})$	$E_T(\{x_i\})$	$E_H(\{x_i\})$	$E_U(\{x_i\})$
0.08	0.015669	0.015755	0.021922	0.462539
0.04	0.008376	0.009074	0.008409	0.301695
0.02	0.006156	0.005366	0.004239	0.165777
0.01	0.003667	0.003044	0.002792	0.117625

TABLE 2. We summarize with an averaged squared error between the discrete solution u_a and the Euclidean distance d with the function $E_a(\{x_i\}) = \frac{1}{10} \sum_{i=1}^{10} (|u_a(x_i) - c_a d(x_i, x_0)|^2)$, and compute this for the different grid sizes h . For the uniform random graph, we additionally average E_U over 10 random graph realizations.

The second viewpoint considers the sets of paths in the graph from the sources to any other node. We define a travel time (over a set of paths) between two nodes and optimize for the minimum arrival time. The final viewpoint assumes a local equation for the travel time to a node from neighbours which have already received the information.

We showed equivalences between these different views, as summarized in Table 1. With these equivalences we are able to (i) use the front propagation model for computation of solutions by exploiting the relationship to fast marching methods (ii) form and solve optimal travel times problems over sets of paths in a network and (iii) relate models on regular grid-like graphs to PDE models. In this framework we provide examples such as a generalization of classical equivalence between optimal paths and Dijkstra's algorithm [11] and in the setting of regular grids that formal limits lead to new families of PDEs.

This investigation lays groundwork for new research directions. From modelling and algorithmic developments, we can apply these results to larger datasets, extending the work of [24] to look at new robust methods for label propagation problems in semi-supervised learning. Our approach may be applied to propagation phenomena such as opinion formation on social networks or consensus in multi-agent systems, where methods such as graph Laplacians, [14, 16, 20] and other distance metrics are typically used. Our framework can also encapsulate control problems such as using s (or w) as a control, thus could be used in applications such as evacuation planning [1]. Fast marching procedures also offer adjoint equations at no additional cost, leading to particularly efficient methods for inverse problems in these settings [8, 12]. Developments in analysis are also possible, as our formal PDE limits in the regular grid setting lead to questions of convergence together with existence and uniqueness theory. Another direction is to extend the theory to random graph constructions (as demonstrated in the numerical results), possibly by applying constructions found [18, 13, 17]. Investigation of properties of the path sets that lead to optimal travel times could also allow new interpretation of results.

ACKNOWLEDGEMENTS

ORAD would like to acknowledge the generous support of Eric and Wendy Schmidt (by recommendation of Schmidt Futures) and the National Science Foundation (grant AGS-1835860). LMK acknowledges support from the the Warwick Research Development Fund through the project ‘Using Partial Differential Equations Techniques to Analyse Data-Rich Phenomena’, the European Union Horizon 2020 research and innovation programmes under the Marie Skłodowska-Curie grant agreement No. 777826 (NoMADS), the Cantab Capital Institute for the Mathematics of Information and Magdalene College, Cambridge (Neville Research Fellowship).

REFERENCES

- [1] V. BAYRAM, *Optimization models for large scale network evacuation planning and management: A literature review*, Surveys in Operations Research and Management Science, 21 (2016), pp. 63–84.
- [2] M. BELKIN, I. MATVEEVA, AND P. NIYOGI, *Regularization and semi-supervised learning on large graphs*, in International Conference on Computational Learning Theory, Springer, 2004, pp. 624–638.
- [3] A. L. BERTOZZI AND A. FLENNER, *Diffuse interface models on graphs for classification of high dimensional data*, Multiscale Modeling & Simulation, 10 (2012), pp. 1090–1118.
- [4] A. BLUM AND S. CHAWLA, *Learning from labeled and unlabeled data using graph mincuts*, in Proceedings of the Eighteenth International Conference on Machine Learning, ICML 2001, San Francisco, CA, USA, 2001, Morgan Kaufmann Publishers Inc., pp. 19–26.
- [5] F. CAMILLI, A. FESTA, AND D. SCHIEBORN, *An approximation scheme for a Hamilton-Jacobi equation defined on a network*, Applied Numerical Mathematics, 73 (2013), pp. 33 – 47.
- [6] F. CAMILLI AND C. MARCHI, *A comparison among various notions of viscosity solution for hamilton-jacobi equations on networks*, Journal of Mathematical Analysis and Applications, 407 (2013), pp. 112 – 118.
- [7] K. DECKELNICK AND C. M. ELLIOTT, *Uniqueness and error analysis for Hamilton-Jacobi equations with discontinuities*, Interfaces and Free Boundaries, 6 (2004), pp. 329–349.
- [8] K. DECKELNICK, C. M. ELLIOTT, AND V. STYLES, *Numerical analysis of an inverse problem for the Eikonal equation*, Numerische Mathematik, 119 (2011), p. 245.
- [9] X. DESQUESNES, A. ELMOATAZ, AND O. LÉZORAY, *Eikonal equation adaptation on weighted graphs: fast geometric diffusion process for local and non-local image and data processing*, Journal of Mathematical Imaging and Vision, 46 (2013), pp. 238–257.
- [10] X. DESQUESNES, A. ELMOATAZ, O. LÉZORAY, AND V.-T. TA, *Efficient algorithms for image and high dimensional data processing using eikonal equation on graphs*, in International Symposium on Visual Computing, Springer, 2010, pp. 647–658.
- [11] E. W. DIJKSTRA, *A note on two problems in connexion with graphs*, Numerische Mathematik, 1 (1959), pp. 269–271.
- [12] O. R. DUNBAR AND C. M. ELLIOTT, *Binary recovery via phase field regularization for first-arrival traveltime tomography*, Inverse Problems, 35 (2019), p. 095004.
- [13] M. M. DUNLOP, D. SLEPČEV, A. M. STUART, AND M. THORPE, *Large data and zero noise limits of graph-based semi-supervised learning algorithms*, Applied and Computational Harmonic Analysis, 49 (2020), pp. 655–697.
- [14] A. ELMOATAZ, X. DESQUESNES, AND M. TOUTAIN, *On the game p -Laplacian on weighted graphs with applications in image processing and data clustering*, European Journal of Applied Mathematics, 28 (2017), pp. 922–948.

- [15] A. ELMOATAZ, O. LEZORAY, AND S. BOUGLEUX, *Nonlocal discrete regularization on weighted graphs: a framework for image and manifold processing*, IEEE transactions on Image Processing, 17 (2008), pp. 1047–1060.
- [16] A. ELMOATAZ, M. TOUTAIN, AND D. TENBRINCK, *On the p -Laplacian and ∞ -Laplacian on graphs with applications in image and data processing*, SIAM Journal on Imaging Sciences, 8 (2015), pp. 2412–2451.
- [17] J. FADILI, N. FORCADEL, AND T. T. NGUYEN, *Limits and consistency of non-local and graph approximations to the eikonal equation*. arXiv:2105.01977.
- [18] N. GARCÍA TRILLOS AND D. SLEPČEV, *Continuum limit of total variation on point clouds.*, Archive for Rational Mechanics & Analysis, 220 (2016), pp. 193 – 241.
- [19] E. MERKURJEV, T. KOSTIC, AND A. L. BERTOZZI, *An MBO scheme on graphs for classification and image processing*, SIAM Journal on Imaging Sciences, 6 (2013), pp. 1903–1930.
- [20] R. OLFATI-SABER, J. A. FAX, AND R. M. MURRAY, *Consensus and cooperation in networked multi-agent systems*, Proceedings of the IEEE, 95 (2007), pp. 215–233.
- [21] J. A. SETHIAN, *Theory, algorithms, and applications of level set methods for propagating interfaces*, Acta numerica, 5 (1996), pp. 309–395.
- [22] J. A. SETHIAN, *Fast marching methods*, SIAM Review, 41 (1999), pp. 199–235.
- [23] V.-T. TA, A. ELMOATAZ, AND O. LÉZORAY, *Adaptation of eikonal equation over weighted graph*, in Scale Space and Variational Methods in Computer Vision, X.-C. Tai, K. Mørken, M. Lysaker, and K.-A. Lie, eds., Springer Berlin Heidelberg, 2009, pp. 187–199.
- [24] M. TOUTAIN, A. ELMOATAZ, AND O. LÉZORAY, *Geometric pdes on weighted graphs for semi-supervised classification*, in 2014 13th International Conference on Machine Learning and Applications, 2014, pp. 231–236.
- [25] X. ZHU, *Semi-supervised learning literature survey*, Tech. Rep. 1530, Computer Sciences, University of Wisconsin-Madison, 2005.